Valveless Pumping at Low Reynolds Numbers

Gabriel Amselem◉,* Christophe Clanet, and Michael Benzaquen◉

Laboratoire d'Hydrodynamique, CNRS, École polytechnique, Institut Polytechnique de Paris, 91120 Palaiseau, France

Pumping at low Reynolds number is a ubiquitously encountered feature, both in biological organisms and engineered devices. Generating net flow requires the presence of an asymmetry in the system, which traditionally comes from geometric flow rectifiers. Here, we study a valveless system of N oscillating pumps in series, where the asymmetry comes not from the geometry but from time, that is, the phase shifts between the pumps. Experimental and theoretical results are in very good agreement. We provide the optimal phase shifts leading to the maximal net flow in the continuous $N \to \infty$ limit. The maximal flow rate is larger by 25% than that of a traditional peristaltic sinusoidal wave, for the same amplitude of actuation. Our results hopefully pave the way for the design of more efficient microfluidic pumps.

I. INTRODUCTION

Pumping at low Reynolds number is a broadly encountered feature, both in nature and engineered systems. On the biological side, insects such as butterflies and mosquitoes feed essentially on liquids such as plant nectar or blood and many rely on the action of one or more muscular pumps to take in their food [1]. On the man-made side, the design of micropumps for MEMS applications started with the seminal work of Smits [2] and continued with the Quake valves that are now ubiquitous in microfluidic designs [3], triggering a large variety of designs [4–7].

In one way or another, these natural and engineered devices rely on the presence of an asymmetry in the system, which is essential to pump at low Reynolds number. Some biological and man-made pump designs rely on valves, a role played by the pharynx in mosquitoes [8–10]. However, valves are prone to mechanical failure and clogging and valveless systems of micropumps have been conceived to make them easier to fabricate and more resilient [5,11]. Their mode of operation relies on geometrically asymmetric elements having flow-rectifying properties. Valveless pumping at low Reynolds number is also prevalent in biology, throughout the animal kingdom: in the early stages of embryonic development of a number of species, the heart consists of two chambers that pump fluid without a valve [12–14].

In this paper, we study experimentally and theoretically a valveless pumping system consisting of N identical contracting pumps in series, operating at low Reynolds number. The system does not contain any flow rectifier

(valveless) and the asymmetry comes not from the built-in geometry but from the phase shifts between the oscillating pumps, i.e., from the dynamics of actuation. The average flow rate through the system is computed from the system geometry and the phases of the oscillating pumps. The theoretical results are in very good agreement with the experiments. We find numerically the phase shifts between the N pumps leading to the maximal flow rate, for arbitrary values of N. When the number of pumps is increased to infinity (continuous limit) and for a given amplitude of deformation, the maximum flow rate obtained is larger by 25% than that of a traditional peristaltic sinusoidal wave. Our results thereby hopefully cut the first turf for more efficient designs of microfluidic pumps.

II. PUMPING WITH TWO PUMPS

A. Experimental setup

The experimental setup consists of silicon tubing of internal diameter $2R = 1.5$ mm (Thermo Scientific TM Sterilin, Thermo Fischer, France), partially filled with silicon oil (Rhodorsil ® 47V1000, kinematic viscosity $\nu = 10^{-3}$ m^2 s^{-1}). Cylindrical wooden rods of diameter 1 cm are placed on computer-controlled syringe pumps (Nemesys, Cetoni GMBH, Germany) and press periodically on the silicon tubing (see Fig. 1). These wooden rods constitute the pumps. The evolution of the tubing diameter at the location of rod i can be approximated as $r_i(t) = R[1 - \frac{\varepsilon}{2} + \frac{\varepsilon}{2}\sin(\omega t + \varphi_i)]$, where ε is the normalized pumping amplitude, ω is the pumping angular frequency, and φ_i is the phase shift of pump i (see Fig. 1). The column of oil of length L_{tot} is imaged at 10 Hz with a CMOS camera (Lt225c, Teledyne Lumenera, Canada) and the position of the oil-air interface is followed over time.
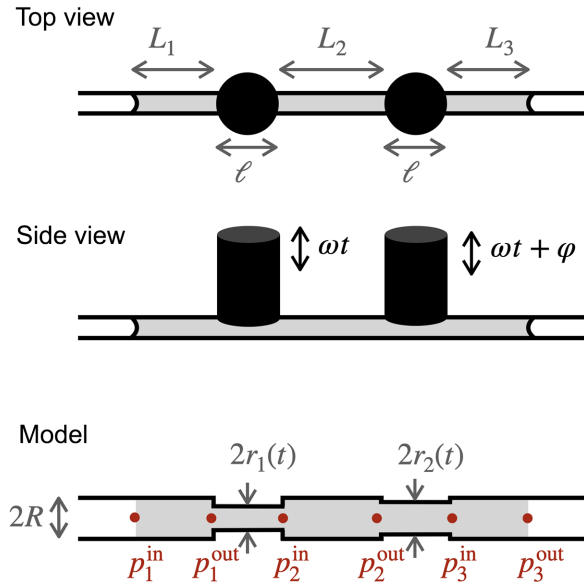
FIG. 1.   A sketch of the experimental setup: two cylindrical wooden rods of diameter 1 cm placed on computer-controlled syringe pumps are used to press periodically on an elastic silicone tubing. The tubing is partially filled with V1000 silicon oil (gray). The parametrization of the system is as follows: two pumps of length ℓ delimit sections of tubing of total length $L_{\text{tot}} = 2\ell + L_1 + L_2 + L_3$. The tubing radius is $R = 0.75$ mm. The varying tubing radius under the pumps is denoted $r_{1,2}(t)$.

When only one pump is actuated, the oil-air meniscus moves periodically and symmetrically left and right at the forcing frequency, leading to on average zero net flow through the system [see Fig. 2(a)]. This is typical of the reversible behavior of flows at low Reynolds number: in the absence of inertia, a symmetric forcing on the fluid does not lead to any net flow [15]. To estimate the value of ε, we measure the length of the column of liquid $L_{\text{tot, 0}}$ in the absence forcing. We then measure its length $L_{\text{tot, max}}$ when a single pump is actuated and maximally pressing on the tube. The resulting effective radius of the deformed cross section is then $r_{\min} = r(1 - \varepsilon)$. By volume conservation, we find that $\varepsilon = 1 - \sqrt{1 - (L_{\text{tot,max}} - L_{\text{tot, 0}})/\ell}$, where $\ell = 1$ cm is the diameter of the wooden rod and hence the size of the pumping region.

When two pumps are actuated, the meniscus still moves periodically left and right at the forcing frequency but in the presence of an additional slower drift. The amplitude and direction of the drift depend on the phase shift $\Delta\varphi = \varphi_1 - \varphi_2$ between the two pumps [see Fig. 2(b)]. The drift velocities of the meniscus are extracted from kymographs of the experiment, for all values of the phase shifts tested. The drift velocity v shows a sinusoidal dependency on the phase shift $\Delta\varphi$ [see Fig. 2(c)], with no drift for $\Delta\varphi = 0, \pm\pi$ and a maximum drift for $\Delta\varphi = \pm\pi/2$. This can be intuitively understood by seeing that when the two pumps are in phase opposition ($\Delta\varphi = \pm\pi$), the fluid

pushed by one pump fills up the space of the tube under the second pump, resulting in a reversible situation and so an absence of net flow. When the phase shift is $\Delta\varphi = \pm\pi/2$, the pump in phase retardation pushes the fluid preferentially away from the other pump, in a discretized version of peristaltic pumping.

B. Theory

The flow generated by the pumps can be calculated under the assumption of small deformations $\varepsilon \ll 1$. Consider the valveless system of two pumps pushing on tubing of radius R and total length L_{tot}, as shown in Fig. 1. The pumps have a length ℓ and the radius of the tubing at the location of the pumps is $r_i(t)$, $i = 1, 2$. The tubing is delimited by the pumps into three sections of length L_1, L_2, and L_3. The total length of the tubing is then $L_{\text{tot}} = L_1 + L_2 + L_3 + 2\ell$. The pressures at the inlet and outlet of the ith section are $p_i^{\text{in}}(t)$ and $p_i^{\text{out}}(t)$, respectively (see the bottom panel in Fig. 1). At low Reynolds numbers and in the cylindrical geometry presented here, flows obey Poiseuille's law, so that the flow rate $Q_i(t)$ in channel i is linked to the pressures $p_i^{\text{in}}(t)$ and $p_i^{\text{out}}(t)$ through

$$\forall i \in [1,3], \quad Q_i(t) = k_i[p_i^{\text{in}}(t) - p_i^{\text{out}}(t)], \quad (1)$$

where $k_i = \pi R^4/8\eta L_i$ is the resistivity of the channel. The flow rates between adjacent channels are related by mass conservation:

$$\forall i \in [1,2], \quad Q_i(t) - Q_{i+1}(t) = 2\ell\pi r_i(t)\partial_t r_i. \quad (2)$$

Lastly, the flow in channel i can be expressed as a function of the resistivity $\kappa_i(t) = \pi r_i(t)^4/8\eta\ell$ of pump $i \in [1,2]$:

$$Q_i(t) = \kappa_i(t)[p_i^{\text{out}}(t) - p_{i+1}^{\text{in}}(t)] + \ell\pi r_i(t)\partial_t r_i. \quad (3)$$

Equations (1)–(3) constitute a linear system of seven scalar equations. The pressures are imposed to be identical at the inlet and outlet of the system: $p_1^{\text{in}} = p_3^{\text{out}} = p_0$. We solve for the seven unknown variables $(Q_1, Q_2, Q_3, p_1^{\text{out}}, p_2^{\text{in}}, p_2^{\text{out}}, p_3^{\text{in}})$, looking for a solution to the equations when the pumps are forced sinusoidally: $r_i(t) = R\left[1 - \frac{\varepsilon}{2} + \frac{\varepsilon}{2}\sin(\omega t + \varphi_i)\right]$.

The time-averaged flow $\bar{Q}_1 = \bar{Q}_2 = \bar{Q}_3 := \bar{Q}$ is found to depend on the phase difference $\Delta\varphi = \varphi_1 - \varphi_2$ between the two pumps through

$$\bar{Q}(\Delta\varphi) = \frac{\pi R^2\ell^2(L_{\text{tot}} - \ell - L_2)}{L_{\text{tot}}^2}\omega\varepsilon^2\sin\Delta\varphi + \mathcal{O}(\varepsilon^3).$$
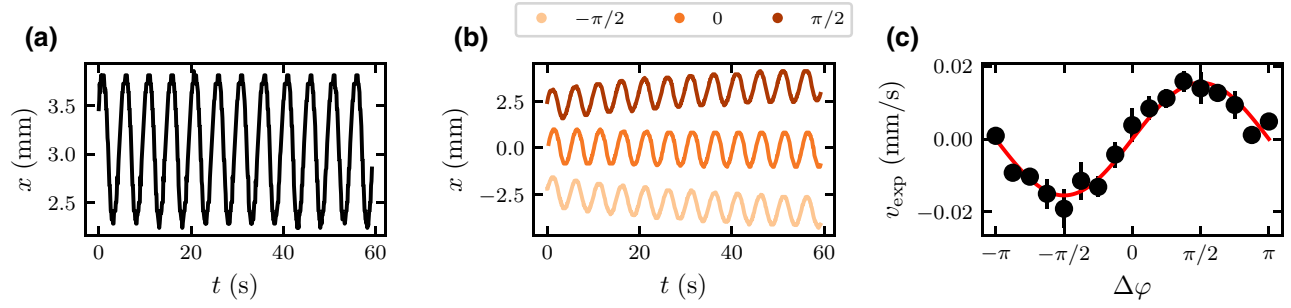
$$(4)$$

FIG. 2.   (a) The oscillating position of the oil-air meniscus when one pump presses periodically on the silicone tubing, with a period $T = 5$ s. (b) When two pumps press periodically on the silicone tubing, the position of the meniscus shows a net drift superposed on oscillations at the forcing period. The drift direction depends on the sign of the phase shift $\Delta\varphi = \varphi_1 - \varphi_2$ between the two pumps. (c) The evolution of the mean drift speed v_{exp} as a function of the phase shift $\Delta\varphi$. The points show experimental data and the line is a fit to a sine function.

The average flow velocity $v_{\text{theor, 2 pumps}} = \bar{Q}/\pi R^2$ in the tubing is then given by

$$v_{\text{theor, 2 pumps}} = (L_{\text{tot}} - \ell - L_2)\frac{\ell^2}{L_{\text{tot}}^2}\omega\varepsilon^2 \sin \Delta\varphi + \mathcal{O}(\varepsilon^3). \quad (5)$$

We recover the experimentally observed dependency of the flow speed on the sine of the phase difference $\sin \Delta\varphi$. The flow speed is proportional to the forcing frequency ω, as can be expected for low-Reynolds-number flows, and depends on a geometric prefactor that involves the ratio of the pump size ℓ to the total length of the fluid column L_{tot}: the larger the fraction of the fluid being pressed by the pumps, the more efficient is the pumping. Note that $\ell = L_{\text{tot}}/2$ at most, for which the flow speed saturates to its maximum value. Lastly, note that pumping is a second-order effect in ε.

C. Comparison between experiments and theory

Experiments are repeated for different values of ε, L_{tot}, and $\Delta\varphi$ and the experimental drift velocities of the oil are plotted as a function of the theoretical velocities in Fig. 3(a). We find good agreement in the scaling between the second-order theory and experiments for small values of $\varepsilon \lesssim 0.2$ [see the dashed line in Fig. 3(a)]. Deviation of the data from the dashed line at larger values of ε indicates that higher-order terms are needed to fully describe the experimental data. Solving the equations of fluid motion up to order $\mathcal{O}(\varepsilon^3)$ and comparing the experiments to the third-order theory gives very good agreement for all parameters tested, up to a numerical prefactor of approximately 1.5 [see Fig. 3(b)]. The expression for the theoretical speed up to third order in ε is given in the Supplemental Material [16].

The fact that the experimental speed is approximately 1.5 times larger than predicted by theory can most likely be attributed to the complex deformation of the tube

when the pumps are actuated. Indeed, under an actuator, the cross section of the tubing does not stay circular but becomes approximately elliptical, which leads to an increased hydrodynamic resistance at the location of the actuator [17]. Such an increased resistance itself leads to a larger pumping efficiency. Moreover, due to elasticity, the deformation of the tubing extends beyond the region of the actuator, which also affects the hydrodynamic resistance of the tube. A discussion of these two effects can be found in the Supplemental Material [16]. Lastly, note that the resistance to flow is inversely proportional to the square of the cross-section area [17] and so a small error in the estimation of ε can lead to large differences in the hydrodynamic resistance.

III. PUMPING WITH $N \geq 3$ PUMPS

A. Three pumps

The theory can be extended to a system of N pumps in series (see below). In particular, for a system of three identical pumps and using the same notation as above, the average flow velocity is found to be

$$v_{\text{theor, 3 pumps}} = \frac{\ell^2}{L_{\text{tot}}^2}\omega\varepsilon^2\big[a_1 \sin(\varphi_1 - \varphi_2) + a_2 \sin(\varphi_1 - \varphi_3)$$
$$+ a_3 \sin(\varphi_2 - \varphi_3)\big] + \mathcal{O}(\varepsilon^3), \quad (6)$$

where the a_i are geometrical prefactors that have the dimension of a length and φ_i is the phase shift of pump i (for the expressions of the a_i, see the Supplemental Material [16]). The validity of this prediction is tested by mounting a system with three pumps, where the forcing amplitude ε, the length of the column of oil L_{tot}, and the phase shifts φ_1 and φ_2 are systematically varied. Again, the experimental results are in good agreement with the theoretical predictions (see Fig. 4). As for the system with two pumps, the experimental velocities for the three-pump
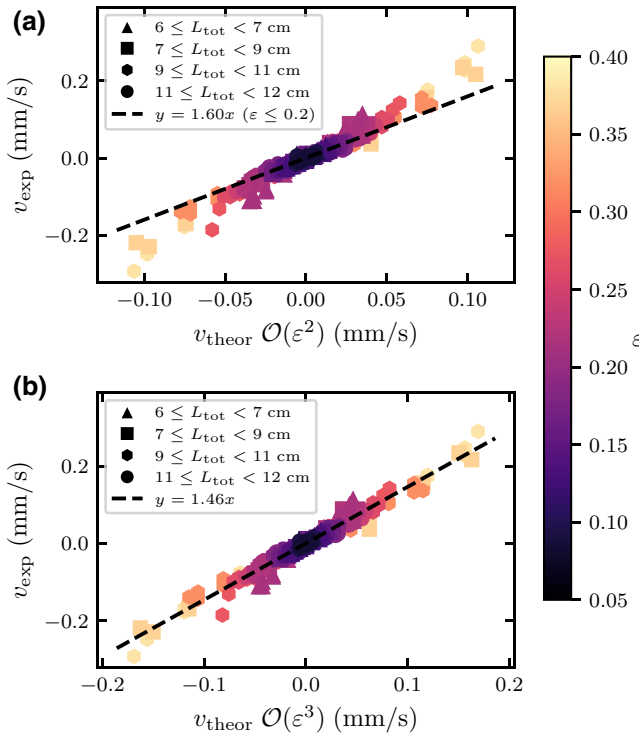
FIG. 3. A comparison between the experimental and theoretical flow speeds (points), for a system of two pumps. The normalized pumping amplitude ε is color coded and the different symbols are for different lengths of the liquid column, L_{tot}. Other parameters: $2R = 1.5$ mm, $l = 1$ cm, and $L_2 = 3$ cm. (a) The experimental versus the theoretical speed calculated up to $\mathcal{O}(\varepsilon^2)$. The dashed line is the best fit to data with $\varepsilon \leq 0.2$. (b) The experimental versus the theoretical speed calculated up to $\mathcal{O}(\varepsilon^3)$. The dashed line is the best fit to all data and shows the line $y = 1.46x$. For a discussion on the existence of a numerical prefactor in the linear fit of the data, see the main text.

device are larger than the theoretical predictions by a factor of approximately 2 (see the black dashed line in Fig. 4), likely for the same reasons as cited above.

B. *N* pumps

Is pumping more efficient when more pumps are added to the system? To answer this question, consider a system of N identical pumps of length ℓ in series, actuated sinusoidally. For simplicity, we now consider that all subsections of the tubing have the same length L and hence the same resistivity $k = \pi R^4/8\eta L$. The total length of the tubing is then $L_{\mathrm{tot}} = N\ell + (N+1)L$. Similarly to Eq. (1)–(3), there are now $3N + 1$ equations to solve in order to compute the flow rate:

$$\forall i \in [1, N+1], \quad Q_i(t) = k[p_i^{\mathrm{in}}(t) - p_i^{\mathrm{out}}(t)]. \quad (7a)$$

$$\forall i \in [1, N], \quad Q_i(t) - Q_{i+1}(t) = 2\ell\pi r_i(t)\partial_t r_i, \quad (7b)$$

$$Q_i(t) = \kappa_i(t)[p_i^{\mathrm{out}}(t) - p_{i+1}^{\mathrm{in}}(t)] + \ell\pi r_i(t)\partial_t r_i. \quad (7c)$$
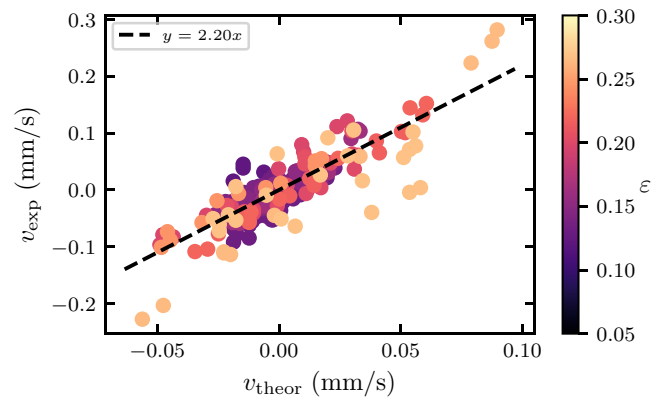

FIG. 4. A comparison between the more than 200 experimental flow-speed values measured and the theoretical speed values (points), for a system of three pumps. The normalized pumping amplitude ε is color coded. The liquid length L_{tot} is varied between 13 and 18 cm. Other parameters: $2R = 1.5$ mm and $l = 1$ cm. The theoretical speed is calculated up to $\mathcal{O}(\varepsilon^2)$, according to Eq. (6). The dashed line is the best fit to all data. The existence of a numerical prefactor between theory and experiment is discussed in the main text.

The same pressure is imposed at the inlet and the outlet ($p_1^{\mathrm{in}} = p_{N+1}^{\mathrm{out}} = p_0$) and the system of equations is solved for the $3N + 1$ unknown variables $(Q_1, \ldots, Q_N, p_1^{\mathrm{out}}, p_2^{\mathrm{in}}, p_2^{\mathrm{out}}, \ldots, p_N^{\mathrm{out}}, p_{N+1}^{\mathrm{in}})$, when the pumps are forced sinusoidally: $r_i(t) = R[1 - \frac{\varepsilon}{2} + \frac{\varepsilon}{2}\sin(\omega t + \varphi_i)]$.

The average flow rate over one period T through a system of N pumps is found to be

$$\bar{Q}(\{\varphi_i\}) = 4\pi R^2 \ell\omega f_N(\varepsilon, b, \{\varphi_i\}) + \mathcal{O}(\varepsilon^3), \quad (8)$$

where we introduce $b = \ell/L$, the ratio of the pump dimension to that of the tubing sections, and

$$f_N(\varepsilon, b, \{\varphi_i\}) = \frac{b}{(Nb + N + 1)^2}$$

$$\times \left(\sum_{M=1}^{N-1}(M(b+1)+1)\sum_{i=1}^{M}\sin(\varphi_i - \varphi_{i+N-M})\right)\varepsilon^2 + O(\varepsilon^3). \quad (9)$$

The flow rate therefore depends on the phase shifts between the pumps and on the aspect ratio $b = \ell/L$; it increases linearly with b for small b and saturates for $b \gg 1$, when the pumps essentially press on the entire length of the tubing.

The phase shifts giving the maximal flow rate for a given aspect ratio b are obtained by solving Eq. (9) numerically, using MATHEMATICA (Wolfram Research, Inc., Illinois). For the particular case of $N = 2$ pumps, the maximum flow rate is obtained for $\Delta\varphi = \pm\pi/2$, independent of the aspect ratio b. For a system of $N \geq 3$ pumps, the optimal phase

shifts depend on the aspect ratio b, albeit only weakly [for $N = 3$ pumps, varying b over 10 orders of magnitude changes the optimal values of the phase shifts by approximately 5% (see Fig. 2 in the Supplemental Material [16])]. Actually, for all tested values of $N \geq 3$, the optimal phases shifts are essentially constant for $b \ll 1$ and $b \gg 1$ and undergo a small variation when the aspect ratio b goes from 0.1 to 10.

We now fix the aspect ratio $b = 1$ as well as the tube size L_{tot} and consider that pumps of size $\ell = L_{tot}/(2N + 1)$ are actuated. The flow rate in the system is then simply given by $\tilde{Q}(\{\varphi_i\}) = \bar{Q}(\{\varphi_i\})/(2N + 1)$. How does the optimal flow rate depend on the number of pumps N? We find that the maximal flow rate in the system $\tilde{Q}_{max}(N)$ increases with the number of pumps N until saturation in the continuous limit ($N \to \infty$) [see the black markers in Fig. 5(a)]. The maximal flow rate in a system of two pumps is approximately 50% as large as in the continuous limit. The increase in the flow rate is very steep when N initially increases: the flow rate in a system of four pumps

is already approximately 80% that of the continuous limit.

Regardless of the number of pumps N in the system, the optimal flow rate $\tilde{Q}_{max}$ is always larger than the flow rate $\tilde{Q}_{sine}$ obtained by naively discretizing a sine wave, for which the phase shifts are equally spaced by $2\pi/N$ [see the orange markers in Fig. 5(a) and the dashed orange line in Fig. 5(b)]. This is most obvious for $N = 2$, where discretizing a sine wave leads to the two pumps being actuated in phase opposition, which does not induce any net flow. For $N = 3$ pumps, the optimal flow rate is approximately 65% larger than $\tilde{Q}_{sine}$ [see the inset in Fig. 5(a)]. The ratio $\tilde{Q}_{max}/\tilde{Q}_{sine}$ decreases when N increases and in the continuous limit, the optimal flow rate is 25% larger than the flow rate obtained with a sinusoidal peristaltic wave [see the difference between the black and orange points in Fig. 5(a) and the inset in Fig. 5(a)].

The wave form leading to the maximal flow rate in the continuous limit is shown in black in Fig. 5(b) for large N, at time $t = 0$. This optimal wave travels along the tube over one period of oscillation. The optimal wave form is different from the traditional sinusoidal peristaltic wave; in particular, the phase values of the first and last pumps are different (see the animated phase profiles in the video in the Supplemental Material [16]).

FIG. 5. (a) Increasing the number of pumps in the system while keeping the tube length constant increases the optimal flow rate $\tilde{Q}_{max}(N)$ (black dots), up to a limit corresponding to the continuous case $N \to \infty$. The optimal flow rate is always larger than the flow rate obtained by naively discretizing a sine wave, where the phase shifts are equally spaced by $2\pi/N$ (orange dots). The inset shows the ratio between the optimal flow rate $\tilde{Q}_{max}(N)$ and the flow rate $\tilde{Q}_{sine}(N)$ obtained by discretizing a sine wave, as a function of N. (b) The wave form leading to the maximum flow in a system of N pumps with $N = 30$. Increasing N further does not change the wave form.

IV. DISCUSSION

The literature on miniaturized pumps, which operate at low Reynolds number, is extremely vast and covers aspects from fluid dispensing in lab-on-a-chip devices for biological analysis [18] to biomedical applications such as microdosing for drug delivery [7]. However, the broad majority of the existing work is concerned with the flow generated by at least three pumps in series, with very few exceptions on pumping with two pumps [19–21]. A physical model of the flow due to pumping with three pumps has been described in Goulpeau *et al.* [22]. In our work, we study in detail the influence of the geometric parameters of the fluidic circuit and of the phase shifts between the pumps, on the flow rate, for $N = 2$ and $N = 3$ pumps and extend the theory of pumping to an arbitrary number N of pumps.

To achieve the highest flow rate possible, existing work usually sets the phase shifts to arbitrary intuitive values and then measures the flow rate as a function of the frequency of actuation of the pumps (see, e.g., Refs. [21,23–26]). At low Reynolds number, however, both quantities are proportional; deviation from proportionality either indicates a change of regime to high Reynolds number or reveals the presence of a compliance in the microsystem, which induces a phase shift between the applied actuation signal and the real mechanical actuation. This difference between the applied actuation and the real actuation is probably at
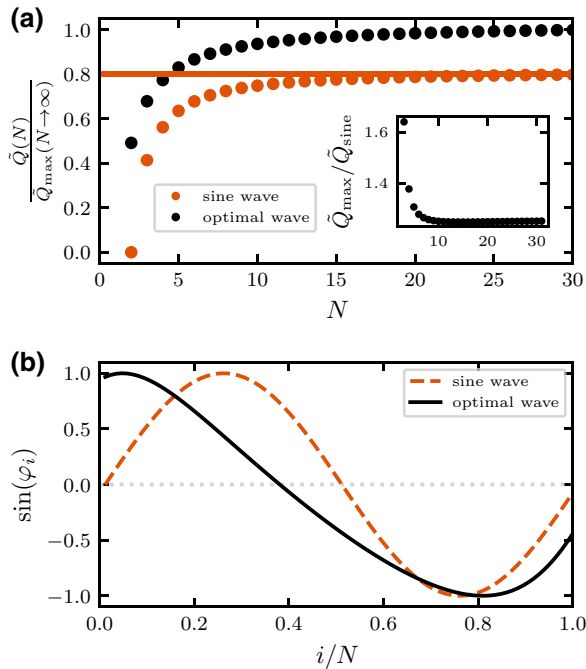
the origin of surprising results, such as obtaining a maximum flow rate in a system of two pumps when they are supposedly actuated in phase ($\Delta\varphi = 0$) or in phase opposition ($\Delta\varphi = \pi$) [21], in direct contradiction to the reversibility of flows at low Reynolds number. Our results show that, in the low-Reynolds-number regime, valveless pumping with two pumps is optimal for phase shifts between the pumps $\Delta\varphi = \pm\pi/2$ and we provide the exact analytical expression of pumping efficiency as a function of the geometric parameters of the problem. The theoretical and experimental results are in good agreement (see Figs. 3 and 4).

The flow due to a simple peristaltic wave traveling along a tube can be analytically calculated (see Refs. [27,28]), with a number of applications. Original ideas making use of peristaltic waves have been put forth, e.g., for the swimming of microorganisms [29,30]. The optimization of peristaltic wave shapes at low Reynolds number has been studied numerically using variational methods [31] and, more recently, boundary integral methods [32]. Here, we obtain numerical results on the optimal peristaltic wave shape at low Reynolds number by studying a system of N discrete pumps and let $N \rightarrow \infty$ (see Fig. 5). The nontrivial optimal peristaltic shape that we find leads to a flow rate larger by 25% than that due to a sinusoidal peristaltic wave. Moreover, in the discrete case of a small number of pumps, the difference between the optimal flow rate and the flow rate obtained by naively discretizing a sine wave is even larger: for $N = 3$ pumps, the optimal flow rate is approximately 65% larger than that obtained with a discretized sine wave.

Note that we find the wave shape leading to the maximal flow rate, considering N pumps actuated at a fixed amplitude ε and with a pump length scaling as $1/N$. Our numerical results indicate that, under these constraints, the energy needed to actuate N pumps with the optimal wave form is larger than for a sinusoidal wave with the same amplitude of pumping ε [see Fig. 4(a) in the Supplemental Material [16]]. For a given energy and relaxing the constraint on the amplitude of pumping, a sinusoidal wave leads to a larger flow than our optimal wave form [see Fig. 4(b) in the Supplemental Material [16]]. In the future, we plan to investigate what the optimal phases and amplitudes of actuation are in a system of N pumps, under the constraint of fixed energy.

Finally, the results presented here are valid for a system of N pumps actuated independently of each other, in a regime where the imposed actuation is instantaneously transmitted to the fluid. They do not take into account effects due to the elasticity of the tubing enclosing the fluid. Elasticity introduces a compliance in the system as mentioned above and can also lead to two neighboring pumps not being independent of each other: if the pumps are too close to each other, the closing of one pump will open the neighboring one. The analysis of such intricate effects is left for future work.

[1] B. J. Borrell and H. W. Krenn, in *Ecology and Biomechanics: A Mechanical Approach to the Ecology of Animals and Plants*, edited by A. Herrel, T. Speck, and N. P. Rowe (CRC Press, Boca Raton, 2006), Chap. 9, p. 185.

[2] J. G. Smits, Piezoelectric micropump with three valves working peristaltically, Sens. Actuators: A. Phys. **21**, 203 (1990).

[3] M. A. Unger, H. P. Chou, T. Thorsen, A. Scherer, and S. R. Quake, Monolithic microfabricated valves and pumps by multilayer soft lithography, Science (New York, NY) **288**, 113 (2000).

[4] D. J. Laser and J. G. Santiago, A review of micropumps, J. Micromech. Microeng. **14**, R35 (2004).

[5] P. Woias, Micropumps—past, progress and future prospects, Sens. Actuators B: Chem. **105**, 28 (2005).

[6] B. D. Iverson and S. V. Garimella, Recent advances in microscale pumping technologies: A review and evaluation, Microfluid. Nanofluidics **5**, 145 (2008).

[7] A. B. Bußmann, L. M. Grünerbel, C. P. Durasiewicz, T. A. Thalhofer, A. Wille, and M. Richter, Microdosing for drug delivery application—A review, Sens. Actuators, A: Phys. **330**, 112820 (2021).

[8] K. Uchida, Cibarial sensilla and pharyngeal valves in *Aedes albopictus* (skuse) and *Culex pipiens* pallens coquillett (Diptera : Culicidae), Int. J. Insect Morphol. Embryol. **8**, 159 (1979).

[9] B. H. Kim, E. S. Seo, J. H. Lim, and S. J. Lee, Synchrotron x-ray microscopic computed tomography of the pump system of a female mosquito, Microsc. Res. Tech. **75**, 1051 (2012).

[10] K. Kikuchi, M. A. Stremler, S. Chatterjee, W. K. Lee, O. Mochizuki, and J. J. Socha, Burst mode pumping: A new mechanism of drinking in mosquitoes, Sci. Rep. **8**, 1 (2018).

[11] E. Stemme and G. Stemme, A valveless diffuser/nozzle-based fluid pump, Sens. Actuators: A. Phys. **39**, 159 (1993).

[12] N. S. Glickman and D. Yelon, Cardiac development in zebrafish: coordination of form and function, Semin. Cell Dev. Biol. **13**, 507 (2002).

[13] E. N. Olson, Gene regulatory networks in the evolution and development of the heart, Science **313**, 1922 (2006).

[14] P. J. Scherz, J. Huisken, P. Sahai-Hernandez, and D. Y. Stainier, High-speed imaging of developing heart valves reveals interplay of morphogenesis and function, Development **135**, 1179 (2008).

[15] E. M. Purcell, Life at low Reynolds number, Am. J. Phys. **45**, 3 (1977).

[16] See the Supplemental Material at http://link.aps.org/supplemental/10.1103/PhysRevApplied.19.024017, which includes Ref. [33], for detailed expressions of the pumping speed, estimates of the tubing deformation and pumping energy, and a video of the optimal wave form.

[17] N. A. Mortensen, F. Okkels, and H. Bruus, Reexamination of Hagen-Poiseuille flow: Shape dependence of the hydraulic resistance in microchannels, Phys. Rev. E **71,** 057301 (2005).

[18] Y. N. Wang and L. M. Fu, Micropumps and biomedical applications—a review, Microelectron. Eng. **195,** 121 (2018).

[19] J. M. Berg, R. Anderson, M. Anaya, B. Lahlouh, M. Holtz, and T. Dallas, A two-stage discrete peristaltic micropump, Sens. Actuators, A: Phys. **104,** 6 (2003).

[20] A. Geipel, A. Doll, P. Jantscheff, N. Esser, U. Massing, P. Woias, and F. Goldschmidtboeing, A novel two-stage backpressure-independent micropump: Modeling and characterization, J. Micromech. Microeng. **17,** 949 (2007).

[21] B. H. Kim, I. C. Kim, Y. J. Kang, J. Ryu, and S. J. Lee, Effect of phase shift on optimal operation of serial-connected valveless micropumps, Sens. Actuators A: Phys. **209,** 133 (2014).

[22] J. Goulpeau, D. Trouchet, A. Ajdari, and P. Tabeling, Experimental study and modeling of polydimethylsiloxane peristaltic micropumps, J. Appl. Phys. **98,** 044914 (2005).

[23] J. Xie, J. Shih, Q. Lin, B. Yang, and Y. C. Tai, Surface micromachined electrostatically actuated micro peristaltic pump, Lab Chip **4,** 495 (2004).

[24] L. S. Jang and W. H. Kan, Peristaltic piezoelectric micropump system for biomedical applications, Biomed. Microdevices **9,** 619 (2007).

[25] G. Liu, C. Shen, Z. Yang, X. Cai, and H. Zhang, A disposable piezoelectric micropump with high performance for closed-loop insulin therapy system, Sens. Actuators, A: Phys. **163,** 291 (2010).

[26] O. Fuchs, Y. Fouillet, S. Maubert, M. Cochet, C. Chabrol, N. David, X. Médal, and R. Campagnolo, A novel volumetric silicon micropump with integrated sensors, Microelectron. Eng. **97,** 375 (2012).

[27] A. Shapiro, M. Jaffrin, and S. Weinberg, Peristaltic pumping with long wavelengths at low Reynolds number, J. Fluid Mech. **37,** 799 (1969).

[28] M. Y. Jaffrin and a. H. Shapiro, Peristaltic pumping, Annu. Rev. Fluid. Mech. **3,** 13 (1971).

[29] A. Ajdari, P.-G. De Gennes, J.-P. Hulin, L. Leibler, and J. Prost, Propulsion péristaltique, Comptes rendus de l'Académie des sciences, Série II, Mécanique, Physique, Chimie, Astronomie **319,** 861 (1994).

[30] A. Ajdari and H. A. Stone, A note on swimming using internally generated traveling waves, Phys. Fluids **11,** 1275 (1999).

[31] S. W. Walker and M. J. Shelley, Shape optimization of peristaltic pumping, J. Comput. Phys. **229,** 1260 (2010).

[32] M. Bonnet, R. Liu, and S. Veerapaneni, Shape optimization of Stokesian peristaltic pumps using boundary integral methods, Adv. Comput. Math. **46,** 1 (2020).

[33] S. Ramanujan, Modular equations and approximations to π, Q. J. Math. **45,** 350 (1914).